SECOND EUROPEAN CONFERENCE ON EARTHQUAKE ENGINEERING
AND SEISMOLOGY, ISTANBUL AUG. 25-29, 2014

SENSITIVITY ANALYSES OF A FRAMED STRUCTURE UNDER SEVERAL TSUNAMI DESIGN-GUIDANCE LOADING REGIMES

Joshua MACABUAG[1], Tiziana ROSSETTO[2], Tristan LLOYD[3],

ABSTRACT

The onshore flow of a tsunami can generate significant loading on buildings and infrastructure leading to various levels of damage or failure. Tsunami building design and tsunami building damage predictions require quantification of these loads. However, there is limited knowledge as to the exact nature of these tsunami loads due to difficulties of obtaining detailed observational data from past tsunami, and limited past experimental and numerical capabilities in reproducing these flows and their interaction with the built environment. This leads to there being a great deal of uncertainty in the spatial and temporal distribution of loads imposed by tsunami on buildings, as well as the magnitude of these loads.

Over recent yeas several design standards have been produced describing tsunami loading of buildings under different loading regimes. This paper aims to show the effect of different loading scenarios and assumptions on structural response by comparing the displacement response obtained when subjecting a simple structure to tsunami loads, defined from design guidance documents in Japan and the USA.

INTRODUCTION

Current tsunami guidelines and recent studies provide equations for the estimation of maximum tsunami loads on buildings as a function of the local building inundation. Whilst various guidelines exist for building design for tsunami loading in the US (FEMA 2008) and Japan (Okada et al. 2004) there are currently no mandatory tsunami building design codes anywhere in the world (G. Chock et al., 2013; Shibayama et al., 2013). Following studies after the 2011 Great East Japan Earthquake and tsunami, there are a number of proposed updates to tsunami-related codes in both the US and Japan being adopted (Chock, Robertson, and Riggs 2013; Fukuyama et al. 2012). However, this is still a subject which has very limited coverage in European guidance despite significant historical tsunamis in Europe.

Whilst design guidance loading aims to give conservative estimates for design, more accurate quantification of loading is required to carry out performance-based tsunami design, detailed damage assessments (e.g. of existing infrastructure), and for the derivation of analytical tsunami fragility functions.

This paper presents a series of 2D analyses of the central bay of an RC framed structure loaded by tsunamis of various heights. The analyses are presented as a series of tsunami pushover curves

[1] EngD Researcher, EPICentre, Department of Civil Environmental and Geomatic Engineering, University College London, Gower Street, London, United Kingdom, WC1E 6BT, joshua.macabuag.12@ucl.ac.uk
[2] Professor, EPICentre, University College London, United Kingdom, WC1E 6BT
[3] PhD Researcher, EPICentre, University College London, United Kingdom, WC1E 6BT

characterizing the structural performance under these tsunami loadings (Figure 9). In order to demonstrate the effect of different loading assumptions on the resulting structural response, static loading regimes from the various studies discussed above will also be considered.

Nomenclature

h = inundation depth (Figure 2), u = flow velocity, z = building elevation above sea-level,
R = maximum tsunami run-up (max height above sea level that tsunami reaches on-land),
$p(y)$ = design tsunami wave pressure at height y above ground, ρ = density, C_d = drag coefficient,
g = acceleration due to gravity, m = mass of debris, Δt = debris impact duration,
a = equivalent inundation depth coefficient (Figure 2),
V_{void} = volume of trapped air voids below the inundation depth,
V_{water} = volume of trapped water on suspended floors,

Tsunami-Induced Building Failure Mechanisms

Various failure mechanisms have been observed in engineered buildings subject to tsunami. There are several methods for grouping building damage (Chock et al. 2013; Fukuyama, Kato, and Ishihara 2013) and some of the most relevant observed failure and damage mechanisms for consideration in analysis and design are summarized in Figure 1 below. The structural analysis carried out in this preliminary study focuses on global lateral displacement of the structure (Figure 1a).

a) Global lateral deflection/failure due to lateral fluid load (hydrostatic and hydrodynamic).

b) Out-of-plane failure of walls due to lateral fluid load (hydrostatic and hydrodynamic).

c) Disproportionate collapse.

d) Foundation failure (overturning, sliding).

Figure 1: Tsunami-induced building failure mechanisms (EEFIT 2011).

Tsunami Forces on Buildings

Analysis of tsunami-induced failure is difficult as there is a great deal of uncertainty in the spatial and temporal distribution of loads imposed by tsunami on buildings, as well as the magnitude of these loads. However, there are various attempts to quantify tsunami-induced loads and damage, which can arise due to hydrostatic forces (lateral fluid pressure, buoyancy, and weight of suspended water), hydrodynamic effects (drag and bore impact) and debris (impact and damming). This preliminary study will consider only fluid flow (ignoring debris) and so hydrodynamic force quantifications prescribed in tsunami design standards will now be examined.

TSUNAMI DESIGN STANDARDS

Tsunami loads recommended in the various design standards presented in this paper are summarized in Table 1. Note that Chilean tsunami design standards are also proposed, but these are largely based on FEMA 646 and so will not be considered separately in this study. Similarly, older standards exist (as outlined by Nistor et al. (2004) but many of these consider only flood loading and all are superseded by those shown in Table 1.

Table 1: Tsunami load components for the various design standards presented in this paper.

Country of Implementation:		**Japan**	**USA**	
Design Standard Title:		**MLIT 2570 (2011)**	**FEMA 646 (2012)**	**ASCE 7-16 (2016)**
Hydro-static	**Lateral hydrostatic pressure**	$\frac{1}{2}\rho g(ah)^2$ See Table 2 below	$\frac{1}{2}\rho g h^2$	$\frac{1}{2}\rho g h^2$
Hydro-dynamic	**Drag**		$\frac{1}{2}C_d\rho(hu^2)_{max}$ See Figure 3 below	$\frac{1}{2}C_d\rho(hu^2)_{max}$
	Bore impact		$1.5F_{drag}$	$\rho\left(\frac{1}{2}gh_b^2 + h_j v_j^2 + g^{1/3}(h_j v_j)^{4/3}\right)$ See Figure 4 below

Tsunami Design Guidance in Japan: MLIT 2570 (2011)

Prior to the 2011 Great East Japan Earthquake and tsunami, Japanese tsunami design guidance took the form of a document titled "Structural Design Method of Buildings for Tsunami Resistance" (SDMBTR) (Okada et al. 2004), which recommends using an equivalent static pressure distribution over a height three times the tsunami inundation depth (Figure 2, Eq. (1), a = 3). The SDMBTR guidelines are based on a study by Asakura et al. (2000) which carried out 84 2-dimensional hydraulic model experiments which measured the pressures exerted on structures positioned at various distances from the sea bed for various wave heights, periods and Froude Numbers (a measure of flow velocity non-dimensionalized by the gravitational wave velocity). The effects of sea walls and other protective barriers were not reviewed in these experiments.

Following the 2011 tsunami a detailed investigative study titled "A study of Improvement of Building Standards etc. in the tsunami critical areas" was carried out by the University of Tokyo Institute of Industrial Science and the Building Research Institute (BRI) under the building standards maintenance promotion program (Tokyo University and BRI 2011). This study used several case-study structures to compare the loading experienced by on-shore structures during the 2011 tsunami (estimated from measured inundation depth at the structure and structural damage levels) to the equivalent hydrostatic loading recommended in SDMBTR.

This review showed that the design wave pressure in SDMBTR generally overestimated the tsunami loading on buildings where they are sheltered from the incoming flow and are further from the shore. The relationships shown in Table 2 are proposed. The 2011 MLIT technical advice document adopts these findings to provide provisional amendments to the 2005 Japan Cabinet Office Tsunami Evacuation Building Guidelines. These proposed amendments were compiled in collaboration with the Housing Bureau and National Institute for Land and Infrastructure Management (NILIM). NILIM and the BRI have continued to develop more detailed guidance recommendations for design of tsunami evacuation structures, as detailed in Fukuyama et al. (2012).

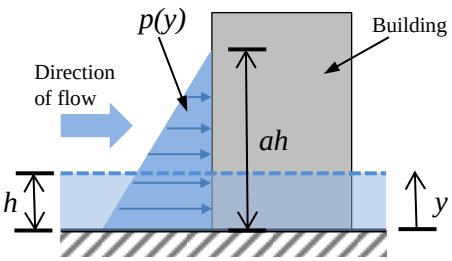

$$p(y) = \rho g(ah - y) \quad (1)$$

Figure 2: Equivalent static loading recommended in MLIT 2570. a is defined in Table 2 below.

Table 2: Tsunami loading coefficient (a) as a function of distance from water source and presence of sheltering structures (Fukuyama et al. 2012; MLIT 2011).

	With shelter between the facility and the incoming wave		**No shelter between the facility and the incoming wave**
Distance from seashore or rivers:	> 500m	< 500m	Any distance
Water depth coefficient *a* (Figure 2)	1.5	2	3

Recommended changes to design guidance include reduction of the tsunami inundation depth coefficient from 3 to the values given in Table 2 below based on distance from the shore and presence of seaward sheltering structures. It is also proposed that wave loading be reduced (by no more than 30 percent) in proportion to openings (e.g. doors and windows) on the pressure-exposed face (note that this appears to ignore the effect of debris damming of openings). Further guidance is also given on the calculation of buoyancy for foundation and superstructure design. Debris and scour are also to be considered, though quantification of these effects is still subject to investigation. For debris it is recommended that progressive collapse following the loss of individual load-bearing elements (e.g. Figure 1c) be designed against. Scour is to be combatted primarily through the use of piles.

Tsunami Design Guidance in USA: FEMA 646 (2012)

The Federal Emergency Management Agency (FEMA) produces several guides for the design and assessment of structures affected by natural hazards. FEMA's Coastal Construction Manual (FEMA, 2000), was first published in 1981, and its current version gives brief guidance for peak tsunami velocities and depth adjustments as part of its coastal flooding sections.

FEMA 646: Guidelines for Design of Structures for Vertical Evacuation from Tsunamis (FEMA 2008) provides guidance for calculating tsunami loads on structures, and provides equations for hydrostatic, hydrodynamic and debris forces. Hydrodynamic forces considered in this preliminary study are shown in Figure 3 (Eq. (2) and Eq. (3)).

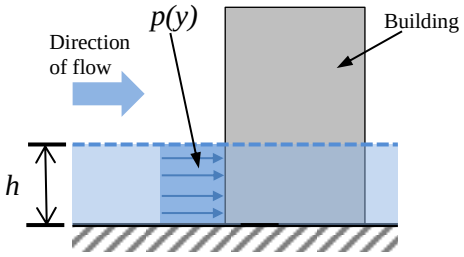

$$F_{impulse} = 1.5 \times F_{drag} \quad (2)$$

$$F_{drag} = \frac{1}{2}\rho_s C_d B (hu^2)_{max} \quad (3)$$

$$(hu^2)_{max} = gR^2\left(0.125 - 0.235\left\{\frac{z}{R}\right\} + 0.11\left\{\frac{z}{R}\right\}^2\right) \quad (4)$$

Figure 3: Uniformly distributed hydrodynamic loading recommended in FEMA 646.

Various studies find that the initial impulsive (bore impact) force can be greater than the drag force on a structure (Lloyd and Rossetto 2012; Nistor et al. 2004; Ramsden 1996; Robertson and Riggs 2011b). The bore impact force is therefore the most onerous lateral fluid load and is simply defined as a multiple of the drag force (Figure 3).

Drag (Equation (2)) is a function of the maximum momentum flux experienced by the structure (hu^2, Eq. (3)). Maximum momentum flux is itself considered a function of maximum tsunami run-up (R) and building elevation (z). Therefore for a given design inundation depth (h) there is not a unique tsunami load, but rather a range of loads defined by the combination of run-up and elevation (Table 3).

It is highlighted that the maximum drag force does not occur at the maximum inundation depth (at which point the theoretical flow velocity is momentarily zero), but at the point at which the momentum flux (hu^2) is a maximum (defined by equation (4)). Therefore, for a given maximum inundation depth at a building, the maximum force occurs at a lower inundation depth than that maximum. However, FEMA 646 states to simply take the maximum force (defined by Equation (3)) and apply it as a uniform vertical pressure distribution over the height of the maximum inundation depth, for conservatism.

On occasions where it is necessary to estimate the velocity of the leading tip of the inundation (where flow depth is theoretically zero, i.e. there is no significant bore), the following relationship is provided (Equation (5)):

$$u_{max} = \sqrt{2gR\left(1 - \frac{z}{R}\right)} \tag{5}$$

Tsunami Design Guidance in USA: ASCE 7-16 (2016)

The current version of American Society of Civil Engineering standard "ASCE 7-10: Minimum Design Loads for Buildings and Other Structures" contains some guidance on loads during flooding but does not contain guidance specifically related to tsunami. The 2016 edition of the ASCE 7 Standard is proposed to contain a new chapter (Chapter 6 – "Tsunami Loads and Effects") which will include loads for tsunami and its effects, and the design procedure will also incorporate certain aspects of Performance Based Tsunami Engineering. Whilst ASCE 7-16 is not yet published, members of the Tsunami Loads and Effects Subcommittee have published several research and conference papers detailing the recommendations that they are proposing to make.

Regarding dynamic lateral fluid loads, drag is to be calculated in a similar way to that recommended in FEMA 646 (Table 1, Chock 2013). However, a different approach to calculating bore impact forces is adopted. The tsunami wave-train often consists of multiple tsunamis and the largest wave is often not the leading wave (e.g. where individual wave celerity exceeds group velocity during deep see propagation meaning that the largest proportion of the tsunami's energy is not carried in the leading waves), and so it is possible for there to be standing water on-shore during a tsunami bore inundation. Bore impact over standing water is to be calculated as shown in Figure 4 below.

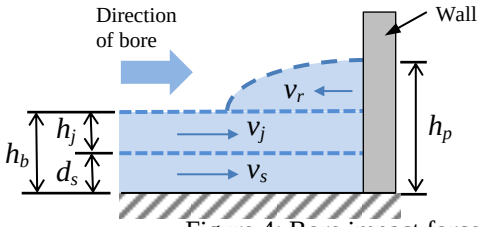

$$F_{bore} = \rho\left(\frac{1}{2}gh_b^2 + h_j v_j^2 + g^{1/3}\left(h_j v_j\right)^{4/3}\right) \tag{6}$$

$$h_r = g^{-\frac{1}{3}}\left(v_j h_j\right)^{\frac{2}{3}} \tag{7}$$

$$v_j = \sqrt{g d_s\left(\frac{1}{2}\left\{\frac{h_b}{d_s}\right\}^2 + \frac{1}{2}\left\{\frac{h_b}{d_s}\right\}\right)} \tag{8}$$

Figure 4: Bore impact forces given in Robertson and Riggs (2011b).

Equations (6) and (7) are derived from conservation of momentum for the control volume shown in Figure 4. Equation (8) is derived from hydraulic jump theory. User-defined unknowns are the standing water depth (d_s), height of hydraulic jump (h_j), and velocity of the standing water (v_s).

It is also stated in Chock (2013) that a simplified pseudo-static approach may be adopted if only maximum tsunami depth at the site can be estimated. A conservative hydrostatic lateral pressure can be applied to the structure to represent the effect of hydrodynamic flow on the structure, determined using the maximum inundation depth with a fluid density of three times that of seawater (Equation (9)):

$$p(y) = (3\rho)gh \tag{9}$$

ANALYSIS OF A STRUCTURE UNDER TSUNAMI LOADING

A series of 2D analyses is carried out of the central bay of an RC framed structure loaded by tsunamis of various heights. This analysis forms the basis of a novel methodology presented here: tsunami pushover analysis.

In order to best illustrate the tsunami pushover procedure this preliminary study will focus on the simple lateral deflection failure mechanism shown in Figure 1a. Additional superstructure and substructure failure mechanisms, as well as effects such as debris impact and preceding seismic damage, will be the focus of further studies.

Structural Model

The RC framed structure analysed is a four-story, 2D bare frame used in a series of full-scale shake-table experiments (A. Pinto et al. 1999). The RC bare frame was designed to be representative of construction practices used in southern European countries in the 1950's and 1960's. RC details are typical of that time, and lateral resistance is low as no specific seismic provisions were included. The FE model used for analysis is shown in Figure 5. Inter-story heights are 2.7m and a slab with 2m on each side is cast together with the beams. Beam dimensions, reinforcement details and material properties are as given in (Carvalho et Al 1999).

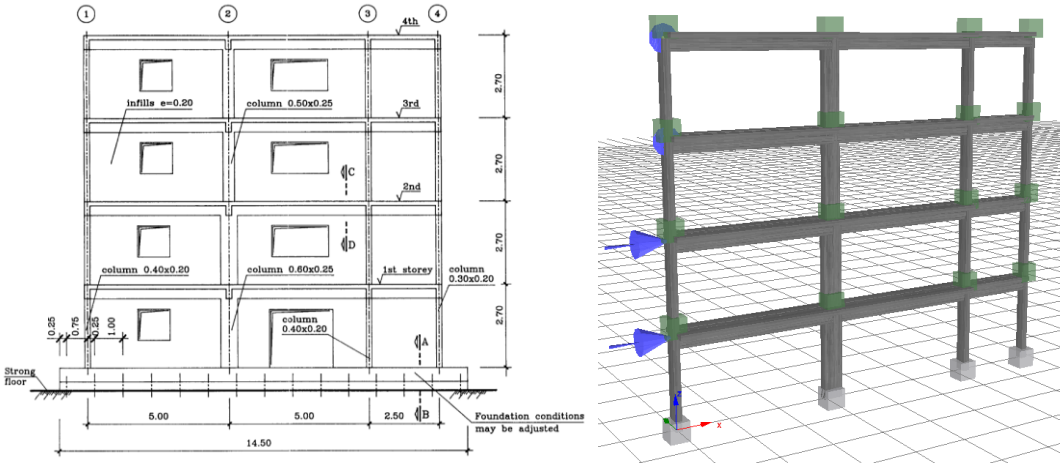

Figure 5: Structural elevation (left. Source: (Carvalho et Al 1999)) and FE model (right) with equivalent nodal forces for a tsunami rising above the 2nd floor.

Loading

Table 3: Load cases used to generate tsunami push-over curves.

Tsunami PO Curve Ref	Guidance Document	Description of Loading	Governing Equation
1	MLIT 2570	Equivalent hydrostatic pressure. No shelter from the incoming wave.	Equation (1), $a = 3$
2	MLIT 2570	Equivalent hydrostatic pressure. >500m from the water source with shelter from the incoming wave.	Equation (1), $a = 2$
3	MLIT 2570	Equivalent hydrostatic pressure. <500m from the water source with shelter from the incoming wave.	Equation (1), $a = 1.5$
4	FEMA 646	Impulse loading based on the maximum momentum flux at each inundation depth. Uniform vertical distribution. Runup taken as that of the maximum credible tsunami at the site, assumed as 10m for the purpose of this investigation.	Equations (2)(3)(4), for each h (h_i): max load defined by $R = R_{max}$ (constant), $z = R_{max} - h_i$
5	FEMA 646	Impulse loading based on the minimum momentum flux at each inundation depth. Uniform vertical distribution.	Equations (2)(3)(4), for each h (h_i): Min load defined by $z = 0$ (constant), $R = h_i$
6	ASCE 7-16	Hydrostatic drag (no bore impact).	Equations (3), (4). $C_d = 2$
7	ASCE 7-16	Simplified pseudo-static approach. Hydrostatic pressure distribution with density multiplied by 3.	Equation (9)
8	ASCE 7-16	Bore impact over a dry bed. At each step of inundation depth (h_i), bore height = 50% of inundation depth.	Equations (5)(6)(7). $h_b = 0.5h_i$
9	ASCE 7-16	Bore impact over standing water. At each step of inundation depth (h_i), bore height = 50% of inundation depth and standing water is assumed to a depth of 15% of the bore height.	Equations (6)(7) (8). $h_b = 0.5h_i$ $h_j = 0.15h_b$

Tsunami pushover analysis is carried out in order to rapidly assess structural performance over a range of tsunami intensities. Tsunami pushover analysis is a novel methodology whereby a structural model is loaded by tsunamis of various heights in order to generate tsunami pushover curves characterizing the structural performance under tsunami loading. The procedure followed is as shown in Figure 6.

The collection of performance points (for tsunamis which give increasing maximum inundation depths) forms the performance curve, or tsunami pushover curve (Figure 9). This procedure is followed for loading regimes specified in the guidance documents MLIT 2570 (MLIT 2011), and FEMA 646 (FEMA 2012), and proposed for ASCE 7-16 (Chock, Robertson, and Riggs 2013; Chock 2013). The loading regimes used are summarized in Table 3.

For determining ASCE 7-16 bore impact forces over dry land it is not possible to use the bore velocity relationship given in Equation (8), as this equation tends to an infinite bore velocity as standing water depths reduce to zero ($\lim_{d_s \to 0} v_j \to \infty$). This demonstrates that Equation (8), which is based on hydraulic jump theory, is not suitable for estimating the velocity of a bore propagating over dry land, as stated in Robertson and Riggs (2011b). Therefore, in order to estimate bore velocity the relationship given in FEMA 646 (Equation (5)) for estimating velocity at the leading tip of a surge has been used instead.

For determining ASCE 7-16 bore impact forces over standing water it is necessary to select values for the unknowns: standing water depth (d_s), height of hydraulic jump (h_j), and velocity of the standing water (v_s). As per Robertson and Riggs (2011a), standing water velocity is taken as zero. Given the very long wavelength of earthquake-induced tsunamis it is unrealistic and over-conservative to consider maximum inundation depth to be fully achieved by the incoming bore, and so the bore height (in both the dry bed and standing water cases) should instead be taken as a proportion of the maximum inundation depth. Similarly, in the absence of detailed inundation data, the depth of standing water will be estimated as a proportion of bore height. For the purpose of comparison with other guidance-document forces the height of the incoming bore has been arbitrarily chosen as 50% of the height of the maximum inundation depth at the structure (h_i), with standing water assumed to a depth of 15% of the bore height. Sensitivity to these parameters is examined in the discussion section below.

Figure 7 shows the input loads calculated as per steps 1 and 2 of Figure 6 for all load cases given in Table 3.

1. Define a maximum inundation depth at the building for a particular tsunami (h_i).
2. Calculate the corresponding static tsunami loading on the building (F_i).
3. Calculate and record the structural response (performance point. E.g. $\delta_{top\_drift\_i}$).
4. Increment the maximum inundation depth and repeat step 1 ($i \rightarrow i+1$).

Figure 6: Calculation procedure used to generate tsunami pushover curves.

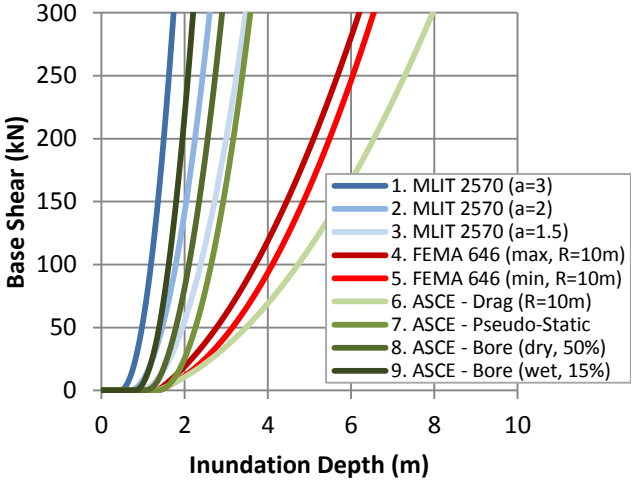

Figure 7: Comparison of Input Loads

The chosen load cases represent distinct and different loading scenarios covering bores, surges and steady flows. Therefore, the purpose of their comparison is not to assess their accuracy, but to highlight the variability in tsunami loading that can be experienced by an onshore structure and to present the range of inputs that will be used in analysis. This variability is increased further when considering the range of assumptions that have been made in deriving these load relationships. Load cases are compared in more detail in the discussion section below. The purpose of this paper is therefore to identify the significance of this variability by analysing a structure's sensitivity to variations in tsunami loading.

Finite Element Analysis

The analysis package chosen for this example application is Seismostruct. This software is chosen due to its ability to simulate large displacement behaviour under static or dynamic loading, considering both geometric and material nonlinearities. Non-linear material behaviour is modelled using the fibre-plasticity approach, whereby each member cross-section is made up of several fibres associated with a uniaxial non-linear stress-strain relationship and the cross-section behaviour is determined by integrating the fibre responses across the section at each calculation step. Fibre-plasticity was chosen over the lumped-plasticity approach as there is no requirement to pre-define plastic hinge locations. Validation of the FE model has been carried out for various seismic analyses and verified against results from physical experiments (Rossetto et al. 2014).

RESULTS

Structural failure occurred via a soft-story mechanism for all loading profiles (Figure 8), induced by failure of ground-to-1st floor columns due to bending (shear stress at column heads was not significant). Figure 8 shows an example of the level of structural damage according to the chosen performance criteria (Table 4), at the calculation step immediately prior to numerical instability of the model. The resulting capacity curves for the structure under the various loading profiles are shown in Figure 9 below. Note that in Figure 9 load cases 1, 2, 3, 7, 8 and 9 all lie on the same curve, as do cases 4 and 5. This is addressed in the discussion section at the end of this paper. Figure 10 shows the Inter-Storey Drift (ISD) ratio vs inundation depth.

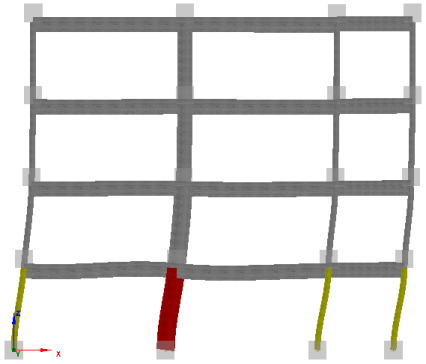

Figure 8: Structure under FEMA 646 loading (δ_{top} = 38mm).

Performance Criteria Description	Material Monitored	Strain Criteria	Colour
Yield	Steel reinforcing bars	ε > 0.0013	Yellow
Spall	Concrete cover	ε > -0.0025	Orange
Crush	Core concrete (contained within rebar)	ε > -0.0031	Red

Table 4: Performance criteria indicated by coloured members in Figure 8.

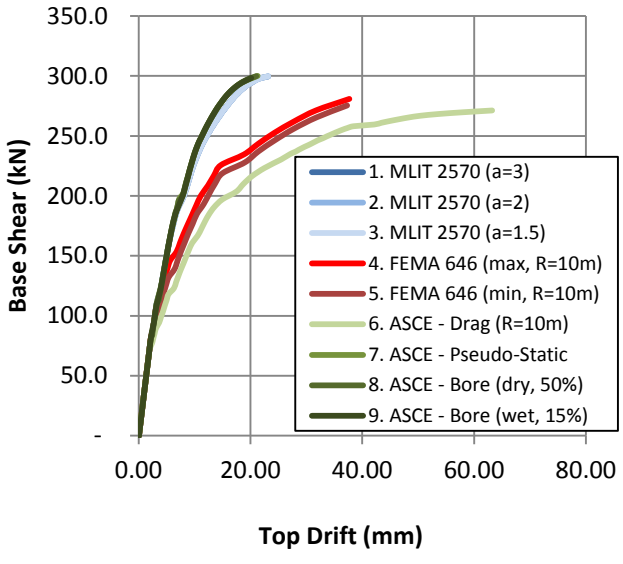

Figure 9: Applied Load vs Top Drift.

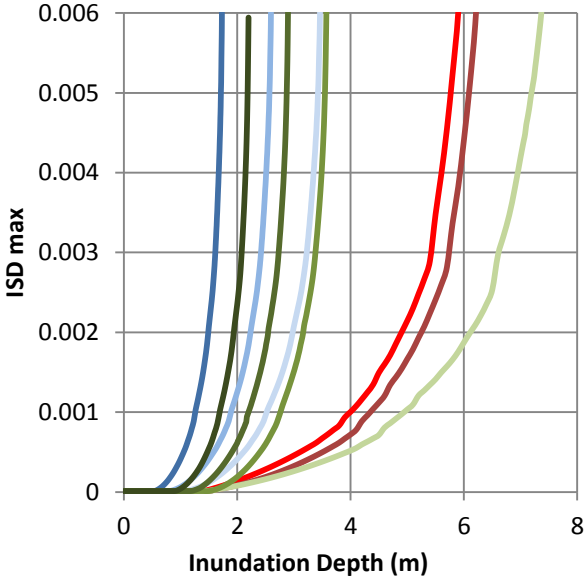

Figure 10: Maximum Inter-Story Drift Ratio vs inundation depth.

DISCUSSION

Design Standard Loading Comparison

It can be seen from Figure 7 that the ASCE 7-16 drag force (load case 6) is the lowest force and corresponds to approximately FEMA/1.5, as expected from Equation (2). MLIT load cases give much higher load estimates than FEMA and the ASCE drag load case at each inundation depth, which agrees with load comparison studies by Yeh, Robertson, and Preuss (2005). For the inundation parameters chosen (h_b=0.5h_i, h_s=0.15h_b): the ASCE load case of a bore impact over standing water (load case 9) is the most onerous ASCE load case and comparable to the MLIT case for unsheltered buildings (load case 1); the ASCE load case of a bore propagating over dry land (load case 8) is comparable to the MLIT case for sheltered buildings within 500m of the shore (load case 2); and the ASCE pseudo-static approach is comparable to the MLIT case for sheltered buildings more than 500m for the shore (load case 3).

The load cases presented in Table 3 define several distinct and different loading scenarios. Table 5 compares the independent variables used by the various guidance documents to define tsunami loading. Figure 11 is a semi-qualitative graphical representation of those scenarios, considering two parameters: the Froude Number (as a parameter considering both velocity and depth), and the blockage ratio (b/W) (as this defines whether flow will be permitted around the structure, or will be reflected back). Both of these parameters are defined in the axis titles of Figure 11.

Table 5: Comparison of input variables used to define tsunami loading under the various loading scenarios.

Guidance Document	Independent Variables
MLIT 2570	h , a
FEMA 646	z , R
ASCE 7-16	h_b , h_j

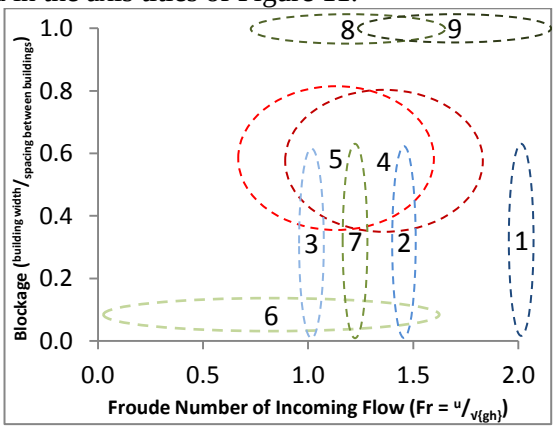

Figure 11: Comparison of loading scenarios flow velocities and blockage ratios.

In order to plot each load case in Figure 11 the following assumptions are made:

The equation for load cases 1, 2 and 3 represents dynamic force but does not expressly allow velocity as an input and therefore correspond to specific Froude Numbers (i.e. velocity is approximated as fixed functions of depth for the three cases). By correlating the proposed equivalent hydrostatic load (Equation (1)) to drag force a correlation between the depth coefficient (a) and Froude Number (Fr) is formed ($Fr = \frac{a}{\sqrt{2}}$, Figure 7b, see Tokyo University and BRI (2011) for derivation). The specified depth coefficients (a) are correlated with building damage data from the 2011 tsunami, where in reality flow was permitted around buildings. Therefore, blockage ratios < 0.6 are assumed in Figure 7b.

Although load cases 4 and 5 are calculated based on the traditional steady-state drag relationship, the factor applied to represent impulsive bore impact loading (Equation (2)) is derived from a series of flume experiments of various blockage ratios, from solid walls to circular columns (Nistor et al. 2004). Figure 11 therefore shows a range of blockage ratios for these load cases.

Load cases 6 is based on the traditional steady-state drag relationship for which flow is permitted around the building such that there is negligible blockage and backflow. A blockage ratio < 0.2 is therefore assumed in Figure 7b.

For the purposes of this preliminary study, load cases 4, 5 and 6 are applied in isolation and so therefore do not account for high blockage cases, where flow around the structure is restricted and there will likely be a significant difference in inundation depth on the front and rear of the structure such that net hydrostatic effects would also become significant. As both depth and velocity can be specified, these relationships can apply over a range of Froude Number flow regimes, as indicated in Figure 7b. Load cases 4 and 5 are approximations of bore impact force calculated as a multiple of drag force, so are more severe than loadcase 6, and so are shown in Figure 7b as applicable for higher Froude Numbers, with load case 4 (a maximum for a given inundation depth) being greater than 5 (a minimum).

Load case 7 represents dynamic force but does not expressly allow velocity as an input and therefore correspond to specific Froude Numbers. If a fixed Froude Number is calculated in a similar manner to that described for the MLIT load cases (cases 1, 2 and 3) then the Froude Number shown in Figure 7b is derived (Fr = 1.22).

Load cases 8 and 9 are derived from experiments with blockage = 1 (a wall which occupies the width of the test flume). Although the reflected return flow is measured to have an average Froude number of approximately Fr = 1, the inflow depth and velocity can be specified and so can apply over a range of Froude Number flow regimes, as indicated in Figure 11.

Calculation of Bore Impact Forces

In order to calculate example bore impact loads (load cases 8 and 9) the parameters of standing water depth (h_s) and height of hydraulic jump (h_j) (and the combination of these values, the total bore height, h_b) have been estimated as a proportion of the inundation depth (h_i). Figure 12 shows the effect of varying these assumed proportions.

Figure 12a shows input loads whereby the bore height (for both dry bed and standing water cases) is taken to be the same as the maximum inundation depth (h_i) at each calculation step, whereas Figure 12b takes bore height to be 50% of the maximum inundation depth. As expected, it can be seen that increasing bore height (h_b) as a proportion of maximum inundation depth (h_i) greatly increases the load experienced by the structure. For a given bore height (h_b), as relative standing water depth (d_s) increases, the jump height (h_j=h_b-d_s) and so load applied decreases. The bore inundating over standing water is generally more onerous than the dry bed case, except where the standing water depth becomes a significant proportion of the total bore height (such as in Figure 12b where, the standing water depth is 50% of the total bore height). Determination of realistic values for these parameters will be the subject of further study.

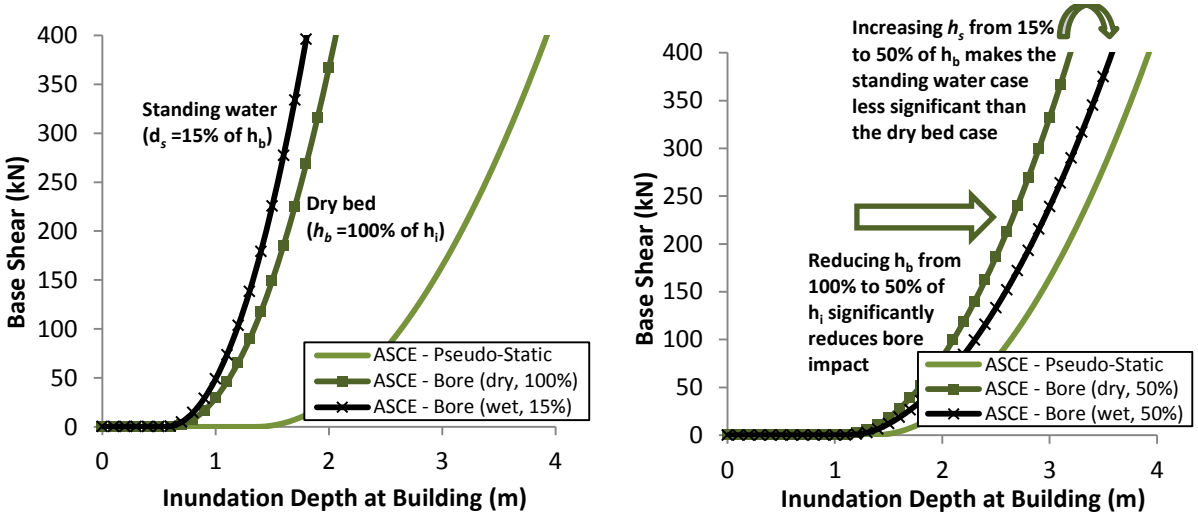

a: Bore height (h_b) = max inundation depth (h_i); Standing water (h_s) = 15% of bore height.

b: Bore height (h_b) = 50% of inundation depth (h_i); Standing water (h_s) = 50% of bore height.

Figure 12: ASCE bore impact parameter sensitivity analysis. The ASCE pseudo-static load (load case 7) is included for comparison purposes.

There is currently no single formula for deriving impact forces for a bore propagating over dry land (load case 8). For the calculation of load case 8 assumptions have therefore been made based on expressions in publications by members of the ASCE 7-16 Tsunami Loads and Effect sub-committee. These formulations may be amended in the final issue of ASCE 7-16, but the analysis presented in this paper provides a preliminary comparison with the other load cases. Note also that bore impact experiments (Robertson and Riggs 2011b) are based on wall impacts where there is no flow around the structure, and where the impacting surface is perpendicular to the direction of the incoming flow. There are currently no expressions for bodies within the flow and for non-bluff bodies.

The Effect of Load Distribution on Structural Response

Figure 9 shows that load cases 1, 2, 3, 7, 8 and 9 (which are all of triangular load distribution) all lie on the same pushover curve, as do cases 4 and 5 (which are of uniform load distribution). Therefore it can be seen that tsunami pushover curves are identical for identical load distributions. However differences become apparent when considering structural deflection as a function inundation depth (Figure 10) rather than base shear. This is due to the very different magnitude of the forces applied for each inundation depth (Figure 7).

The tsunami pushover curves (Figure 9) show that for a given level of base shear the structure deflects least under triangular load distributions and most under uniform load distributions. This can be explained by considering the height of the centroid of the applied loading based on the respective loading distributions. The height of the centroid of the applied load was greatest for the uniform load distributions and least for triangular distributions. Considering the structure to deflect approximately as a vertical cantilever fixed at the base, these centroidal loading positions would account for the differences in top drift shown in Figure 9.

The Effect of Structural Response Variations on Damage Predictions

The differences shown in Figure 10 highlight that the resultant damage predictions will be different, depending on the loading regime used (Macabuag and Rossetto 2014). This highlights that pushover analysis for accurate damage predictions requires the loading applied to be as realistic as possible (in terms of both magnitude and distribution) for each inundation depth, and so simplified and conservative loading defined for design purposes may not provide the required accuracy.

To ascertain the validity of using design standard forces for damage predictions it will be necessary to compare these results with those using more detailed time-history forces from physical experiments (Robertson and Riggs 2011b; Rossetto et al. 2011). Work carried out by Lloyd and Rossetto (2012) on laboratory-generated long-wave experiments is producing expressions for tsunami load time-histories based on inundation parameters. However, existing guidance does not discuss how to apply tsunami load time-histories to structures and assess a building's response from the structural analysis.

CONCLUSION

This paper has shown the effect of different loading assumptions on structural response by comparing the displacement response obtained when subjecting a simple structure to tsunami loads, defined from design guidance documents in Japan and the USA. The following conclusions can be drawn:

- There is a large variation in the tsunami loading recommended in design standards. Japanese design standards (MLIT 2570) prescribe the most conservative loading, though similar in magnitude to bore impact forces prescribed in ASCE 7-16.
- Bore impact loading prescribed in ASCE 7-16 is significantly greater than drag forces. The load magnitude is sensitive to standing water depth levels, which may only be obtained from very accurate inundation models.
- Load relationships need to be developed for bores propagating over dry land, bodies which experience flow around the structure, and non-bluff bodies. Long-wave experiments conducted by Lloyd and Rossetto (2012) are producing these preliminary relationships.

REFERENCES

A. Pinto, G. Verzeletti, J. Molina, and H. Varum. 1999. *Pseudo-Dynamic Tests on Non-Seismic Resisting RC Frames (ICONS)*.

Asakura, R., K. Iwase, T. Ikeya, M. Takao, T. Kaneto, N. Fujii, and M. Omori. 2000. "Experimental Research on Wave Power of Tsunami Surged over the Land beyond the Upright Seawalls (in Japanese)." *Coastal Engineering Journal, , Japan Society of Civil Engineering* No.47: 911–15.

Carvalho et Al. 1999. *Preparation of the Full-Scale Tests on Reinforced Concrete Frames – Definition of the Specimens, Loads and Testing Conditions – ICONS Topic 2*.

Chock, Gary Y.K. 2013. "Development of Tsunami Structural Design Provisions for the USA." In *10th International Conference on Urban Earthquake Engineering,*.

Chock, Gary Y.K., Ian N Robertson, DL Kriebel, Mathew Francis, and Ioan Nistor. 2013. *Tohoku, Japan, Earthquake and Japan of 2011: Performance of Structures under Tsunami Loads*. ASCE.

Chock, Gary Y.K., Ian Robertson, and H. Ronald Riggs. 2013. "Tsunami Structural Design Provisions for a New Update of Building Codes and Performance-Based Engineering." In *ASCE 2011 Solutions to Coastal Disasters 2011 SOLUTIONS TO COASTAL DISASTERS 2011*, , 423–35.

EEFIT. 2011. "Field Report: Earthquake and Tsunami of 11th March 2011." (March).

FEMA. 2008. *Fema 646: Guidelines for Design of Structures for Vertical Evacuation from Tsunamis*. http://www.fema.gov/library/viewRecord.do?id=3463.

———. 2012. "FEMA 646: Guidelines for Design of Structures for Vertical Evacuation from Tsunamis." (April).

Fukuyama, Hiroshi, Hiroto Kato, and Tadashi Ishihara. 2013. "Categorization of Damage to Buildings Caused by the 3.11 Tsunami." In *14th U.S.-Japan Workshop on the Improvement of Structural Design and Construction Practices*, , 1–8. https://www.atcouncil.org/files/ATC-15-13/Papers/03_FUKUYAMApaper.pdf.

Fukuyama, Hiroshi, Hiroto Kato, Tadashi Ishihara, Seitaro Tajiri, Masanori Tani, Yasuo Okuda, Toshikazu Kabeyasawa, and Yoshiaki Nakano. 2012. "Structural Design Requirement on the Tsunami Evacuation Buildings." In *14th U.S.-Japan Workshop on the Improvement of Structural Design and Construction Practices*, http://www.nehrp.gov/pdf/UJNR_2013_Tsunami_Manuscript.pdf.

Lloyd, T O, and T Rossetto. 2012. "A Comparison between Existing Tsunami Load Guidance and Large-Scale Experiments with Long-Waves ." In *15 World Conference on Earthquake Engineering*,.

Macabuag, Joshua, and Tiziana Rossetto. 2014. "Towards the Development of a Method for Generating Analytical Tsunami Ragility Functions." In *2nd European Conference on Earthquake Engineering and Seismology*,.

MLIT. 2011. *Further Information Concerning the Design Method of Safe Buildings That Are Structurally Resistant to Tsunamis - Technical Advice No. 2570.pdf*.

Nistor, Ioan, Dan Palermo, Younes Nouri, and Tad Murty. 2004. "Tsunami-Induced Forces on Structures." In *Handbook of Coastal and Ocean Engineering*, ed. Young C Kim. World Scientific Publishing Co. Pte. Ltd, 261 – 286. http://www.scribd.com/doc/77272681/3/Tsunami-Induced-Forces-on-Structures.

Okada, T, T Sugano, T Ishikawa, T Ohgi, S Takai, and C Hamabe. 2004. *Structural Design Method of Buildings for Tsunami Resistance*. http://www.bcj.or.jp/src/c06_course/bltr/2004/bltr465.pdf.

Ramsden, Jerald D. 1996. "FORCES ON A VERTICAL WALL DUE TO LONG WAVES , BORES , AND DRY-BED SURGES." *Journal of W* (JUNE): 134–41.

Robertson, Ian N, and H. Ronald Riggs. 2011a. "DRAFT OMAE2011-49487 TSUNAMI BORE FORCES ON WALLS." In *Proceedings of the ASTM 2011 30th Internal Conference on Ocean, Offshore and Arctic Engineering*, , 1–9.

———. 2011b. "OMAE2011-49487 Tsunami Bore Forces on Walls." In *Proceedings of the ASTM 2011 30th Internal Conference on Ocean, Offshore and Arctic Engineering*,.

Rossetto, Tiziana, William Allsop, Ingrid Charvet, and David I. Robinson. 2011. "Physical Modelling of Tsunami Using a New Pneumatic Wave Generator." *Coastal Engineering* 58(6): 517–27. http://linkinghub.elsevier.com/retrieve/pii/S0378383911000135 (November 25, 2012).

Rossetto, Tiziana, Pierre Gehl, Stylianos Minas, Arash Nassirpour, Joshua Macabuag, Philippe Duffour, and John Douglas. 2014. "Sensitivity Analysis of Different Capacity Approaches to Assumptions in the Modelling, Capacity and Demand Representations." In *International Conference on Vulnerability and Risk Analysis and Management*,.

Shibayama, Tomoya, Miguel Esteban, Ioan Nistor, Hiroshi Takagi, Nguyen Danh Thao, Ryo Matsumaru, Takahito Mikami, Rafael Aranguiz, Ravindra Jayaratne, and Koichiro Ohira. 2013. "Classification of Tsunami and Evacuation Areas." *Natural Hazards* 67(2): 365–86. http://link.springer.com/10.1007/s11069-013-0567-4 (July 1, 2013).

Tokyo University, and BRI. 2011. *Interim Report of the Building Standards Improvement Promotion Project No.40, A Study of Improvement of Building Standards Etc in the Tsunami Critical Areas*. http://www.mlit.go.jp/common.

Yeh, H., I. Robertson, and J. Preuss. 2005. *Development of Design Guidelines for Structures That Serve as Tsunami Vertical Evacuation Sites*. http://nctr.pmel.noaa.gov/tsu400/documents/Course_3_Day_3/Session_8/ofr05-4.pdf.